Pancreatology 21 (2021) 912–919

Contents lists available at ScienceDirect

Pancreatology

journal homepage: www.elsevier.com/locate/pan

Important role of Nfkb2 in the Kras^{G12D}-driven carcinogenesis in the pancreas

Zonera Hassan [a], Christian Schneeweis [a], Matthias Wirth [b], Sebastian Müller [c], Claudia Geismann [d], Thorsten Neuß [a], Katja Steiger [e, f], Oliver H. Krämer [g], Roland M. Schmid [a], Roland Rad [c, f], Alexander Arlt [d, h], Maximilian Reichert [a, f, i], Dieter Saur [f, j], Günter Schneider [a, f, *]

[a] Medical Clinic and Polyclinic II, Klinikum rechts der Isar, Technical University Munich, 81675, München, Germany
[b] Department of Hematology, Oncology and Tumor Immunology, Campus Benjamin Franklin, Charité - Universitätsmedizin Berlin, Hindenburgdamm 30, 12203, Berlin, Germany
[c] Institute of Molecular Oncology and Functional Genomics, Technical University Munich, 81675, München, Germany
[d] Laboratory of Molecular Gastroenterology and Hepatology, 1st Department of Internal Medicine, University Hospital Schleswig-Holstein, 24105, Kiel, Germany
[e] Institute of Pathology, Technische Universität München, 81675, München, Germany
[f] German Cancer Research Center (DKFZ) and German Cancer Consortium (DKTK), 69120, Heidelberg, Germany
[g] Department of Toxicology, University of Mainz Medical Center, 55131, Mainz, Germany
[h] University Department for Gastroenterology, Klinikum Oldenburg AöR, European Medical School (EMS), 26133, Oldenburg, Germany
[i] Center for Protein Assemblies (CPA), Technische Universität München, 85747, Garching, Germany
[j] Institute for Translational Cancer Research and Experimental Cancer Therapy, Technical University Munich, 81675, München, Germany

A R T I C L E I N F O

Article history:
Received 29 January 2021
Received in revised form
11 March 2021
Accepted 17 March 2021
Available online 26 March 2021

Keywords:
NFκB2
Kras
Pancreatic cancer

A B S T R A C T

Background: Oncogenic Kras initiates and drives carcinogenesis in the pancreas by complex signaling networks, including activation of the NFκB pathway. Although recent evidence has shown that oncogenic gains in *Nfκb2* collaborate with Kras in the carcinogenesis, no data at the level of genetics for the contribution of *Nfκb2* is available so far.
Methods: We used *Nfkb2* knock-out mice to decipher the role of the gene in Kras-driven carcinogenesis *in vivo*.
Results: We show that the *Nfkb2* gene is needed for cancer initiation and progression in Kras^{G12D}-driven models and this requirement of *Nfkb2* is mechanistically connected to proliferative pathways. In contrast, *Nfκb2* is dispensable in aggressive pancreatic ductal adenocarcinoma (PDAC) models relying on the simultaneous expression of the *Kras* oncogene and the mutated tumor suppressor p53.
Conclusions: Our data add to the understanding of context-dependent requirements of oncogenic Kras signaling during pancreatic carcinogenesis.

Introduction

Pancreatic ductal adenocarcinoma (PDAC) is initiated and driven by the *KRAS* oncogene and mutations in this oncogene occur in over 90% of cases. Oncogenic KRAS orchestrates signaling networks including several major pathways like the RAF/mitogen-activated protein kinase kinase (MEK)/extracellular signal-regulated kinase (ERK)-, and the phosphoinositide-3-kinase (PI3K)/AKT-pathways [1–4]. In 2018, we described a link of an increased gene-dosage of mutant KRAS to tumor progression [5], an observation detected also in the human disease [6]. In addition, we identified oncogenic gains in *Myc*, *Yap1*, and *Nfκb2* to collaborate with oncogenic KRAS, placing a particular interest on these genes [5].

NFκB2 (p100/p52), together with NFκB1 (p105/p50), RelA/p65, RelB, and Rel composes the NFκB family of transcription factors [7–9]. The IκB kinase (IKK) complex, containing IKK1, IKK2, and NEMO/IKKγ, controls NFκB signaling. Inflammatory cytokines activate canonical NFκB signaling by inducing the N-terminal

* Corresponding author. Technische Universität München, Klinikum rechts der Isar, Medical Clinic and Polyclinic II, Ismaninger Str. 22, 81675, Munich, Germany.
E-mail address: guenter.schneider@tum.de (G. Schneider).

https://doi.org/10.1016/j.pan.2021.03.012
1424-3903/

phosphorylation of inhibitor of κB (IκB) proteins, leading to their ubiquitination and proteasomal degradation. Consequently, the classical NFκB dimer p50-RelA is released and translocates to the nucleus to activate transcription. In alternative NFκB signaling, NIK (MAP3K14) activates IKK1. Subsequently, IKK1 phosphorylates NFκB2 leading to its ubiquitylation and subsequent proteasomal processing of p100 to p52. Upon processing the alternative dimer, p52-RelB enters the nucleus to activate NFκB targets [7–9].

NFκB signaling contributes to the pathobiology of PDAC development and maintenance [10–15]. In genetically engineered mouse models (GEMMs) of PDAC, $Kras^{G12D}$ activates the NFκB signaling pathway [16,17]. Considering alternative NFκB signaling, proteasomal degradation of TRAF2 stabilizes NIK in PDAC cell lines to induce this branch of the pathway [18]. In addition, the glycogen synthase kinase 3α (GSK-3α) was shown to control non-canonical NFκB signaling in PDAC [19]. Control of proliferation by the alternative NFκB signaling pathway is described in PDAC models [18–21].

Instructed by the *Nfkb2* genetic gains in murine PDAC models and the relevant expression in human PDAC [5], we hypothesized that *Nfkb2* is important for the carcinogenesis in the pancreas. Therefore, we used *Nfkb2* knock-out mice to investigate the role of the gene in murine PDAC models with variable aggressiveness. We show that *Nfkb2* is connected to proliferative pathways that drive the carcinogenesis in the pancreas, a role that is bypassed by the mutated tumor suppressor p53.

Material & methods

Mouse lines

The *Nfkb2* knock-out mouse line was described [22] and the following genotyping primers were used: wildtype *Nfkb2*: p52 _In1 Up 5′ G T C C T C C A C G C T G G C T G A A A 3′; p52_Exon2 LP 5′ A G A T C C G G T G G A G G T C G A G A T 3′; *Nfkb2* knock-out: NeoT2 5′ C C A C G A C G G C G T T C C T G G 3′; Neo Rev 2 5′ C C C A T T C G C C A A G C T C T T C A G 3′. *Ptf1a*^{Cre}, *Pdx1-Cre*, *LSL-Kras*^{G12D}, and *LSL-p53*^{R172H} mouse lines, the genotyping strategies, and primers have been described [23–26]. All animals were on a mixed *C57Bl/6*;*129S6/SvEv* genetic background, male and female mice were analyzed, and fed with a standard chow diet purchased from altromin (#1314M, Lage, Germany). Mouse studies were conducted in compliance with European guidelines for the care and use of laboratory animals and were approved by the Institutional Animal Care and Use Committees (IACUC) of the Technische Universität München and Regierung von Oberbayern.

Histochemistry and immunohistochemistry

For histopathological investigations, murine tissues were fixed in 4% formaldehyde (Carl Roth, Karlsruhe, Germany), embedded in paraffin and subsequently sectioned (1.5 μm thick). Sections were stained with hematoxylin and eosin (H&E) as described [27]. For alcian blue staining, paraffin-embedded sections were dewaxed and rehydrated. The slides were incubated in 1% aqueous alcian blue solution (pH 2.5) for 5 min, washed, counterstained for 5 min with nuclear fast red and mounted in Pertex (Leica Biosystems, Wetzlar, Germany). For immunohistochemistry (IHC), formalin-fixed and paraffin-embedded sections were dewaxed, rehydrated and subsequent placed in a microwave (2 min, 800 W and 9 min/360 W) in order to recover antigens. Slides were left at room temperature for at least 20 min and washed with PBS/0.1% Tween. Endogenous peroxidase activity was inhibited by incubation in 3% H_2O_2 for 10 min. Sections were washed with PBS/0.1% Tween and blocked for 1 h at room temperature with 5% serum and 10% Avidin solution (Avidin/Biotin Blocking Kit Vector Laboratories Burlingame, CA, 94010) in PBS. Then, sections were incubated with the following primary antibodies: Ki-67 (1:50) (Sp6; # KI681C01; DCS Innovative Diagnostic System, Hamburg), Cyclin D1 (1:250) (Sp4; RM9104-S Lab vision, Fremont, CA (USA), and Nfkb2 (1:250) (c-5, sc-7386, Santa Cruz Biotechnology, Dallas, TX, USA). Afterwards, secondary antibody conjugated to biotin (1:500, Vector Laboratories, Burlingame, CA) were used. Streptavidin conjugated to peroxidase was utilized with 3,3′-diaminobenzidine tetrahydrochloride (DAB; Sigma-Aldrich) for visualization. Slides were counterstained with hematoxylin, dehydrated and mounted in Pertex. High resolution images were captured by using the microscope Axio Imager.A1 with Axio Cam HRc and analyzed using AxioVision 4.8 software (Carl Zeiss, Jena, Germany). Slides were scanned with Aperio Image Scanner and images were captured by Aperio ImageScope #12.3.0.5056 (Leica Biosystem, Nußloch, Germany).

Quantification and counting of acinar to ductal metaplasia (ADM) and pancreatic intraepithelial neoplasia (PanIN) lesions

For quantification of ADM and PanIN lesion at each time point at least four animals per genotype were analyzed. Three individual H&E stained slides per pancreas (at intervals of 100 μm) were analyzed. Whole sections were counted for the presence of ADMs and PanIN lesions and a 100-fold magnification was used. Mean number of lesions per field for each animal is shown. Identification of ADM and PanIN lesions was performed according to Ref. [28]. For quantification of alcian blue stainings, pancreas of three animals per genotype were investigated. Three stained whole section slides (at intervals of 100 μm) were analyzed using a 100-fold magnification. Mean number of lesions (ADMs and PanINs) per field for each animal is shown. For analysis of Ki-67 and Ccnd1 expression in ADM and PanIN lesions in age-matched mice tissue, 3 animals per genotype were used. For Ki-67 quantification, three slides per animal and for Ccnd1 one slide per animal were analyzed. Depicted is the percentual fraction of Ki-67/Ccnd1-positive ADM or PanIN cells to all counted ADM or PanIN cells.

Cell lines

Establishment of murine pancreatic cancer cell lines from genetically engineered $Kras^{G12D}$-driven mouse models was described [29]. Cell lines were cultured in DMEM medium (#D5796, Sigma-Aldrich Chemie GmbH, Munich) supplemented with 10% fetal calf serum (FCS) (Merck Millipore/Biochrom, Berlin, Germany) and with 1% (w/v) penicillin/streptomycin (Life technologies). Identity of the murine pancreatic cancer cell lines was verified using genotyping PCR. Cell lines were tested for Mycoplasma contamination by a PCR-based method [30].

Protein lysates and western blot

For whole-cell extracts (WCE), cells or tissue were lysed in RIPA buffer (50 mM Tris HCl, 150 mM NaCl, 2 mM EDTA, 1% Triton ×100, 1% Sodium deoxycholate, 0.1%SDS, pH 7.5) supplemented with protease and phosphatase inhibitors (Protease inhibitor cocktail complete EDTA free, Roche Diagnostics, Mannheim, Germany and Phosphatase-Inhibitor-Mix I, Serva, Heidelberg, Germany). Extracts were normalized for protein in protein loading buffer (45.6 mM Tris-HCl pH 6.8, 2% SDS, 10% glycerol, 1% β-mercaptoethanol, 0.01% bromophenol blue) and heated at 95 °C for 5 min. Equal protein amounts (60 μg) were loaded on 10% SDS-polyacrylamide gels and proteins were transferred to Immobilon-FL or nitrocellulose membranes (Merck-Millipore). Membranes were blocked in blocking buffer (5% skim milk and 0.1% Tween in PBS) and incubated in the following primary antibodies: Nfkb2 (4882, dilution:1:1000, Cell Signaling Technology, Danvers, MA, USA), Cyclin D1 (72-13G, sc-450, dilution: 1:250, Santa Cruz Biotechnology, Dallas, TX, USA), β-Actin (#A5316, dilution 1:10000, Sigma-Aldrich, München, Germany), GAPDH (ACR00PT) (Acris GmbH, Herford, Germany, dilution: 1:10000). DyLight™ 680 or 800 conjugated secondary antibodies (1:10000 dilution) (Cell Signaling Technology) were used for detection with a Odyssey Infrared Imaging System (Licor, Bad Homburg, Germany). The system, assuring signals in the linear range, was also used to quantify western blot signals.

Quantitative reverse-transcriptase PCR

Total RNA was isolated from murine pancreas using the Maxwell®16 Total RNA Purification Kit (Promega, Mannheim, Germany), following the manufacturer's instructions. Quantitative analysis of mRNA expression was performed using real-time PCR analysis system (TaqMan, PE StepOnePlus™, Real time PCR System, Applied Biosystems Inc., Carland, CA, USA). SYBR Green Master Mix (ThermoFisherScientific, Darmstadt, Germany) was used as a fluorescent DNA binding dye. Primers are as follows: *Nfκb2* forward: 5′ T G G A A C A G C C C A A A C A G C 3′; reverse: 5′ C A C C T G G C A A A C C T C C A T 3′; mPcna-TM-for1: 5′ G C A A G T G G A G A G C T T G G C A 3′; mPcna-TM-rev1: 5′ A G G C T C A T T C A T C T C T A T G G T T A C 3′; beta-actin forward: 5′ G T C G A G T C G C G T C C A C C 3′; beta-actin reverse: 5′ G T C A T C C A T G G C G A A C T G G T 3′; mGapdh-FW-qPCR: 5′ G G G T T C C T A T A A A T A C G G A C T G C 3′; mGapdh-RV-qPCR: 5′ T A C G G C C A A A T C C G T T C A C A 3′. Raw data were analyzed with Stepone™ software (Applied Biosystem, Inc., Carland, CA, USA) and the ΔΔCt method was used.

RNA-seq analysis, visualization, Hallmark-analysis

mRNA was extracted as described above. RNA quality control and sequencing were done by the genomics and proteomics core facility of the DKFZ Heidelberg (approximately 25M reads/sample (single-end reads); Illumina HiSeq 2000). NGS data were analyzed using the Galaxy platform as described recently [26]. RNA-Seq Data were deposited in the European Nucleotide Archive (ENA) with the accession number: PRJEB30882. Hallmark gene sets of the MolecularSignatureDatabase were used to analyze enriched pathways. Genes regulated with a log2FC $\geq \pm 1$ and Benjamini adjusted p-value <0.05 were analyzed. False discovery rate q values were depicted and all shown q values were <0.05. Heat maps were generated by ClustVis using variance scaling for rows [31].

Statistical methods

ANOVA or two-sided Student's *t*-test was used to investigate statistical significance, as indicated. *p < 0.05, **p < 0.01, ***p < 0.001, and ****p < 0.0001. Kaplan-Meier curves were generated using GraphPad Prism6 and analyzed by log-rank test. p-values were calculated with GraphPad Prism6 and corrected according to Bonferroni for multiple testing. Unless otherwise illustrated, all data were determined from at least three independent experiments or three animals. The data are presented as mean and standard deviation (SD).

Results

Nfkb2 is required for PanIN progression and PDAC development in a Kras^{G12D}-driven PDAC model

Although we have recently linked gains in *Nfκb2* to PDAC development and described the relevant expression of Nfκb2 in human PDAC [5], no functional *in vivo* data, investigating the role of *Nfκb2* are available so far. Therefore, we analyzed *Nfκb2* mRNA expression in a GEMM for the disease. Compared to wildtype pancreas, *Nfκb2* mRNA is increased in the pancreas of six months old *Ptf1a*$^{Cre/+}$;*LSL-Kras*$^{G12D/+}$ (KC^{Ptf}) mice (Fig. 1A). To test the contribution of the *Nfκb2* gene to the Kras^{G12D}-driven

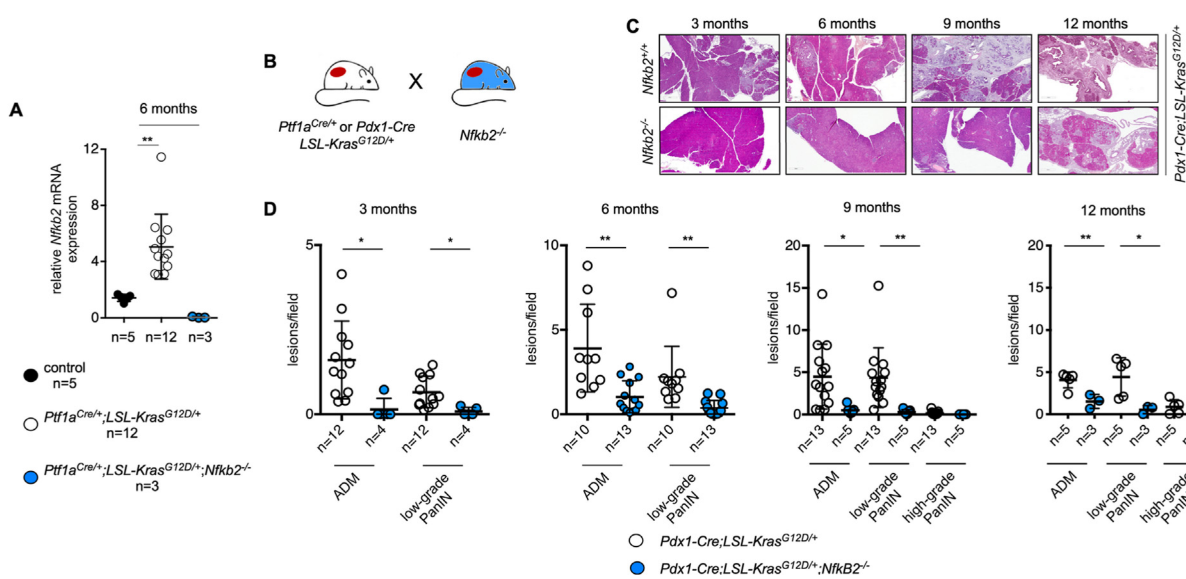

Fig. 1. *Nfκb2 is induced by Kras^{G12D} and mediates PanIN progression in Pdx1-Cre;LSL-Kras$^{G12D/+}$* mice.
A Quantitative PCR analysis of *Nfκb2* mRNA in wild type (black dots), *Ptf1a*$^{Cre/+}$;*LSL-Kras*$^{G12D/+}$ (white dots), and *Ptf1a*$^{Cre/+}$;*LSL-Kras*$^{G12D/+}$;*Nfκb2* $^{-/-}$ (blue dots) mice. Number of animals, analyzed at 6 months of age, is indicated. Shown is the mean ± SD. **p value of a one-way ANOVA <0.01. **B** Illustration of the mouse lines used to analyze the *Nfκb2* gene in the carcinogenesis in the pancreas. Blue color should symbolize the complete knock-out of *Nfκb2*. **C** Representative H&E sections of three, six, nine, and twelve months old *Pdx1-Cre;LSL-Kras*$^{G12D/+}$ and *Pdx1-Cre;LSL-Kras*$^{G12D/+}$; *Nfκb2* $^{-/-}$ mice (Scale bar: 400 μm). **D** Quantification of ADM, low-grade lesions (PanIN-1A and PanIN-1B), and high-grade lesions (PanIN-2/3) in three, six, nine, and twelve months old *Pdx1-Cre;LSL-Kras*$^{G12D/+}$ (white dots), and *Pdx1-Cre;LSL-Kras*$^{G12D/+}$; *Nfκb2* $^{-/-}$ (blue dots) mice. Number of analyzed animals is indicated. Shown is the mean ± SD. p value of a two-tailed unpaired *t*-test *<0.05, **<0.01.

carcinogenesis in the pancreas, we used a *Nfκb2* knock-out mouse line [22]. We crossed *Nfκb2*$^{-/-}$ mice to *Pdx1-Cre;LSL-Kras*$^{G12D/+}$ (KC^{Pdx}) and KC^{Ptf} mice (Fig. 1B). *Nfκb2* knock-out mice were identified by genotyping (SFig. 1A) and lack of *Nfκb2* expression was documented at the mRNA level by qPCR (Fig. 1A) as well as by immunohistochemistry (IHC) (SFig. 1B). In KC models, oncogenic *Kras* induces acinar to ductal metaplasia (ADMs), which progress to murine low and high grade pancreatic intraepithelial neoplasia (mPanIN) and murine PDAC. Compared to KC^{Pdx} mice, we observed a clear deceleration in ADM development and PanIN progression of *Pdx1-Cre;LSL-Kras*$^{G12D/+}$*;Nfκb2*$^{-/-}$ mice (KC^{Pdx}N$^{-/-}$) (Fig. 1C). Quantification of neoplastic lesions over a time course of twelve months demonstrated the impact of the *Nfkb2* gene on ADM development and PanIN progression in KC^{Pdx}N$^{-/-}$ mice (Fig. 1D). Due to tumor suppressive functions of *Ptf1a* [32,33], KC^{Ptf} mice develop mPanINs more aggressively. However, also in this model the profound effect of *Nfκb2* towards ADM and mPanIN development was evident (Fig. 2A). One *Nfκb2* allele is sufficient for normal ADM and PanIN development (Fig. 2A). Using alcian blue staining to visualize the high acidic mucin content of PanINs demonstrated a clear reduction of these lesions in age matched pancreata of KC^{Ptf}N$^{-/-}$ mice (Fig. 2B and C) and this effect is also evident at later time points of disease progression (SFig. 2A). At six months of age, a significant reduction in ADMs and PanIN lesions was observed (Fig. 2D). Kras^{G12D} increases the weight of the pancreas [25], a characteristic that is significantly decreased in KC^{Ptf}N$^{-/-}$ mice (SFig. 2B). To test whether decelerated PanIN progression is translated to impaired mPDAC formation, we determined cancer incidence at 12 months of age. Here, 55% of KC^{Pdx} mice revealed invasive cancer, whereas no PDAC was observed in KC^{Pdx}N$^{-/-}$ mice (Fig. 2E). Median survival of KC^{Ptf}N$^{-/-}$ mice is 468 days (Fig. 2F) and these mice develop mPDAC. The observed median survival is congruent with the median

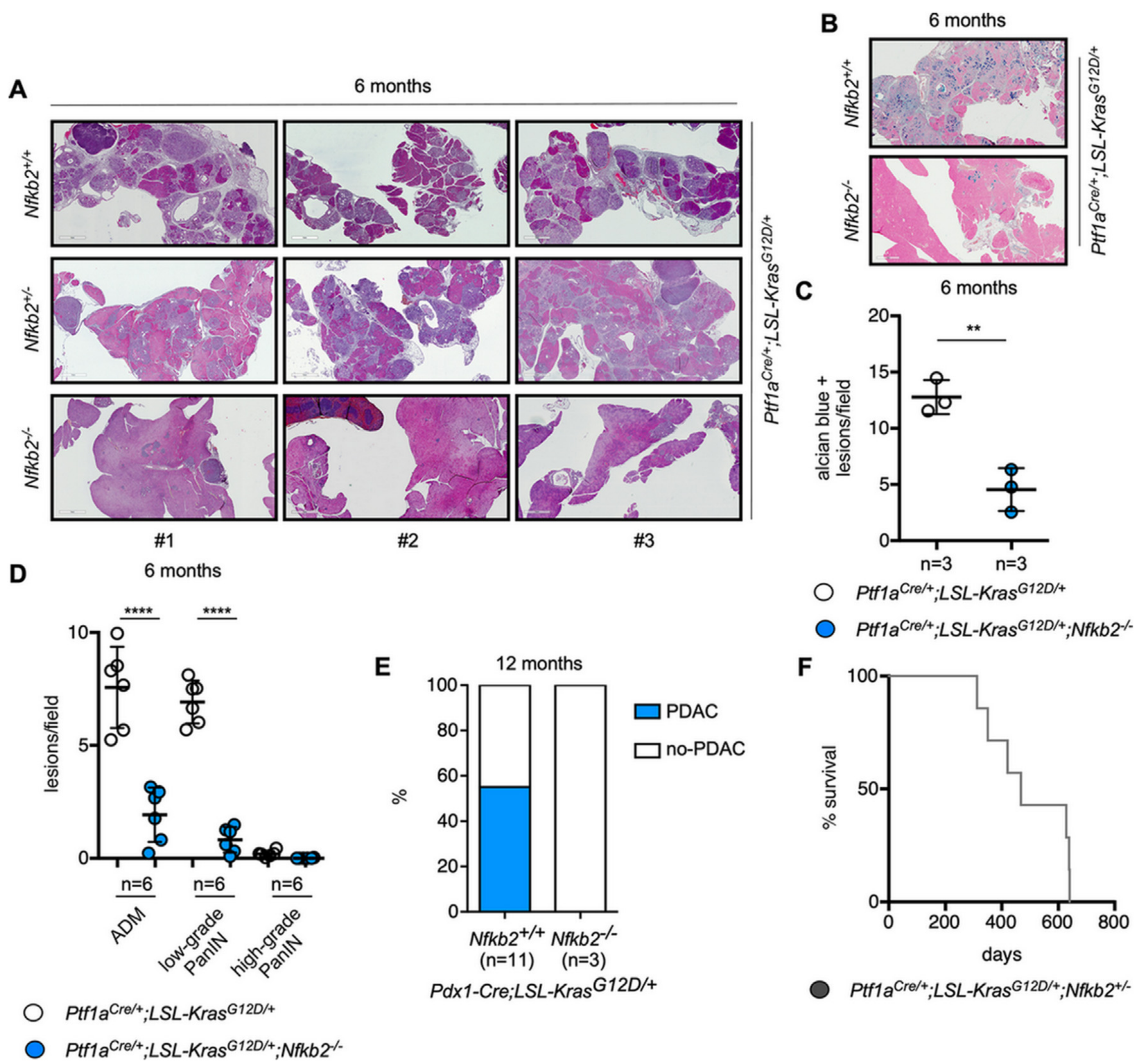

Fig. 2. *Nfκb2 mediates PanIN progression in Ptf1a*$^{Cre/+}$*;LSL-Kras*$^{G12D/+}$ mice.
A Representative H&E sections of three six old month *Ptf1a*$^{Cre/+}$*;LSL-Kras*$^{G12D/+}$, *Ptf1a*$^{Cre/+}$*;LSL-Kras*$^{G12D/+}$*; Nfκb2* $^{+/-}$, and *Ptf1a*$^{Cre/+}$*;LSL-Kras*$^{G12D/+}$*; Nfκb2* $^{-/-}$ mice (Scale bar: 1 mm). **B** Alcian Blue staining of six months old *Ptf1a*$^{Cre/+}$*;LSL-Kras*$^{G12D/+}$ and *Ptf1a*$^{Cre/+}$*;LSL-Kras*$^{G12D/+}$*; Nfκb2* $^{-/-}$ mice (Scale bar: 1 mm). **C** Quantification of alcian blue positive lesion per field of three *Ptf1a*$^{Cre/+}$*;LSL-Kras*$^{G12D/+}$ and three *Ptf1a*$^{Cre/+}$*;LSL-Kras*$^{G12D/+}$*; Nfκb2* $^{-/-}$ mice. Shown is the mean ± SD. p value of a two-tailed unpaired *t*-test **<0.01. **D** Quantification of ADM, low-grade lesions (PanIN-1A and PanIN-1B), and high-grade lesions (PanIN-2/3) in six *Ptf1a*$^{Cre/+}$*;LSL-Kras*$^{G12D/+}$ (white dots), and six *Ptf1a*$^{Cre/+}$*;LSL-Kras*$^{G12D/+}$*; Nfκb2* $^{-/-}$ (blue dots) mice. Number of analyzed animals is indicated. Shown is the mean ± SD. p value of a two-tailed unpaired *t*-test *<0.05, **<0.01. **E** Cancer incidence (% of animals with (blue) or without (white) PDAC) of eleven to twelve-months-old *Pdx1-Cre;LSL-Kras*$^{G12D/+}$ and three *Pdx1-Cre;LSL-Kras*$^{G12D/+}$*;Nfκb2* $^{-/-}$ mice. **F** Kaplan-Meier Blot of seven *Ptf1a*$^{Cre/+}$*;LSL-Kras*$^{G12D/+}$*;Nfkb2*$^{+/-}$ mice. Median survival was 468 days.

survival of our published KC^{Ptf} control cohort (466 days) [25,27] and argues that one *Nfκb2* allele is sufficient to allow PDAC development. No PDAC-related deaths of KC^{Ptf}N$^{-/-}$ mice investigated in between 300 and 525 days of age were detected. Together, these data show that *Nfκb2* is involved in ADM development and PanIN progression.

Nfκb2 contributes to Kras^{G12D}-induced proliferation

A common function of alternative NFκB-signaling is to contribute to the proliferation of cancer cells [34]. To investigate a proliferative role of Nfκb2, we first investigated the fraction of Ki67 positive ADMs and PanIN cells. The proliferation index was significantly decreased in KC^{Ptf}N$^{-/-}$ mice (Fig. 3A and B), an observation also valid in ADM cells of KC^{Pdx}N$^{-/-}$ mice (Fig. 3C), validating the contribution of Nfκb2 to the *Kras^{G12D}*-driven proliferation across models. Coincidingly, the mRNA expression of the proliferative marker gene *Pcna* was reduced in the pancreas of KC^{Pdx}N$^{-/-}$ mice (Fig. 3D). To further corroborate the connection to the cell cycle, we analyzed Ccnd1 expression using immunohistochemistry. Decreased Ccnd1 staining intensity and a decreased fraction of Ccnd1 positive ADM and PanIN cells were detected in KC^{Ptf}N$^{-/-}$ mice (Fig. 3E and F). In addition, tissue western blots of Ccnd1 showed a decreased expression of this cell cycle regulator (Fig. 3G and H). In sum, *Nfκb2* is connected to Kras^{G12D}-driven proliferation and the expression of PCNA and Ccnd1 in the model investigated.

Hallmark signatures linked to Nfκb2

To find genes, pathways and networks controlled by *Nfκb2*, we performed RNA-seq analysis. To avoid a potential bias due to fundamental different disease progression in KC^{Pdx} and KC^{Pdx}N$^{-/-}$ mice, we used an early time point of the disease. Microscopically, the histomorphology of the pancreas of KC^{Pdx} and KC^{Pdx}N$^{-/-}$ mice is in large part normal at four weeks of age. Since we used bulk tissue, we cannot assign regulated genes to a specific cellular compartment. H&E staining of the pancreata used for RNA preparations analyzed by RNA-seq are depicted in Fig. 4A. RNA-seq showed the lack of the expression of exons 1–9 of the *Nfκb2* gene, which were targeted in the *Nfκb2* knock-out mouse line (Fig. 4B) [22]. In Fig. 4C, the top 50 differentially expressed genes in KC^{Pdx} and KC^{Pdx}N$^{-/-}$ mice are shown. Using the Molecular Signature Database (MSigDB; Hallmark gene sets), we detected loss of signatures connected to the pro-proliferative E2F transcription factors, the control of G2/M phase of the cell cycle, adipogenesis, pancreatic beta cells, and angiogenesis in KC^{Pdx}N$^{-/-}$ mice (Fig. 4D). The loss of E2F- and G2M-signatures furthermore corroborate the connection of alternative NFκB-signaling to proliferation. Signatures for mTORC1, p53, the unfolded protein response, the estrogen response, and STAT signaling were enriched in the pancreas of KC^{Pdx}N$^{-/-}$ mice (Fig. 4D).

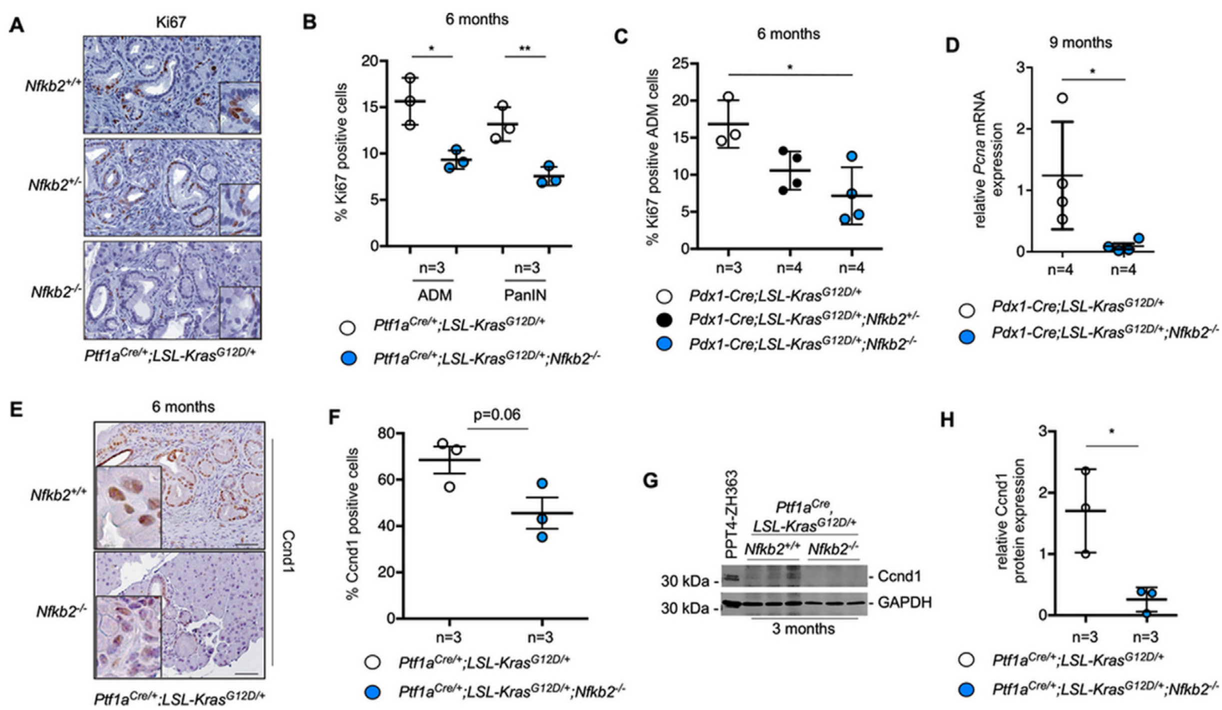

Fig. 3. *Nfκb2 is connected to proliferation of ADMs and PanIN cells.*
A Ki67 immunohistochemistry in six-months old *Ptf1a$^{Cre/+}$;LSL-Kras$^{G12D/+}$*, *Ptf1a$^{Cre/+}$;LSL-Kras$^{G12D/+}$;Nfκb2 $^{+-}$*, and *Ptf1a$^{Cre/+}$;LSL-Kras$^{G12D/+}$; Nfκb2 $^{-/-}$* mice (Scale bar: 50 μm). **B** Quantification of Ki67 positive ADM and PanIN cells in six months old *Ptf1a$^{Cre/+}$;LSL-Kras$^{G12D/+}$* and *Ptf1a$^{Cre/+}$;LSL-Kras$^{G12D/+}$; Nfκb2 $^{-/-}$* mice. Number of mice analyzed in each genotype is indicated. Shown is the mean ± SD. p value of a two-tailed unpaired *t*-test *<0.05, **<0.01. **C** Quantification of Ki67 positive ADM in *Pdx1-Cre;LSL-Kras$^{G12D/+}$*, *Pdx1-Cre;LSL-Kras$^{G12D/+}$;Nfκb2 $^{+/-}$*, and *Pdx1-Cre;LSL-Kras$^{G12D/+}$;Nfκb2 $^{-/-}$* mice. Number of analyzed animals is indicated. Shown is the mean ± SD. p value of a two-tailed unpaired *t*-test *<0.05. **D** Quantitative PCR analysis from pancreatic tissue of *Pcna* mRNA in *Pdx1-Cre;LSL-Kras$^{G12D/+}$* and *Pdx1-Cre;LSL-Kras$^{G12D/+}$; Nfκb2 $^{-/-}$* mice. Number of animals, analyzed at 9 months of age, is indicated. Shown is the mean ± SD. *p value of a two-tailed unpaired *t*-test *<0.05. **E** Ccnd1 immunohistochemistry in six months old *Ptf1a$^{Cre/+}$;LSL-Kras$^{G12D/+}$* and *Ptf1a$^{Cre/+}$;LSL-Kras$^{G12D/+}$; Nfκb2 $^{-/-}$* mice. (Scale bar: 50 μm). **F** Quantification of Ccnd1 positive ADM and PanIN cells in six months old *Ptf1a$^{Cre/+}$;LSL-Kras$^{G12D/+}$* and *Ptf1a$^{Cre/+}$;LSL-Kras$^{G12D/+}$; Nfκb2 $^{-/-}$* mice. Number of animals, analyzed at 6 months of age, is indicated. Shown is the mean ± SD. *p value of a two-tailed unpaired *t*-test is indicated. **G** Ccnd1 western blot in three aged matched (3 months) *Ptf1a$^{Cre/+}$;LSL-Kras$^{G12D/+}$* and *Ptf1a$^{Cre/+}$;LSL-Kras$^{G12D/+}$; Nfκb2 $^{-/-}$* mice. The murine PDAC cell line PPT4-ZH-363 served as a control. GAPDH: equal loading control. **H** Quantification of G. The Ccnd1/GAPDH ratio was determined. The ratio, determined in one *Ptf1a$^{Cre/+}$;LSL-Kras$^{G12D/+}$* mouse, was arbitrary set to 1. Shown is the mean ± SD. *p value of a two-tailed unpaired *t*-test *<0.05.

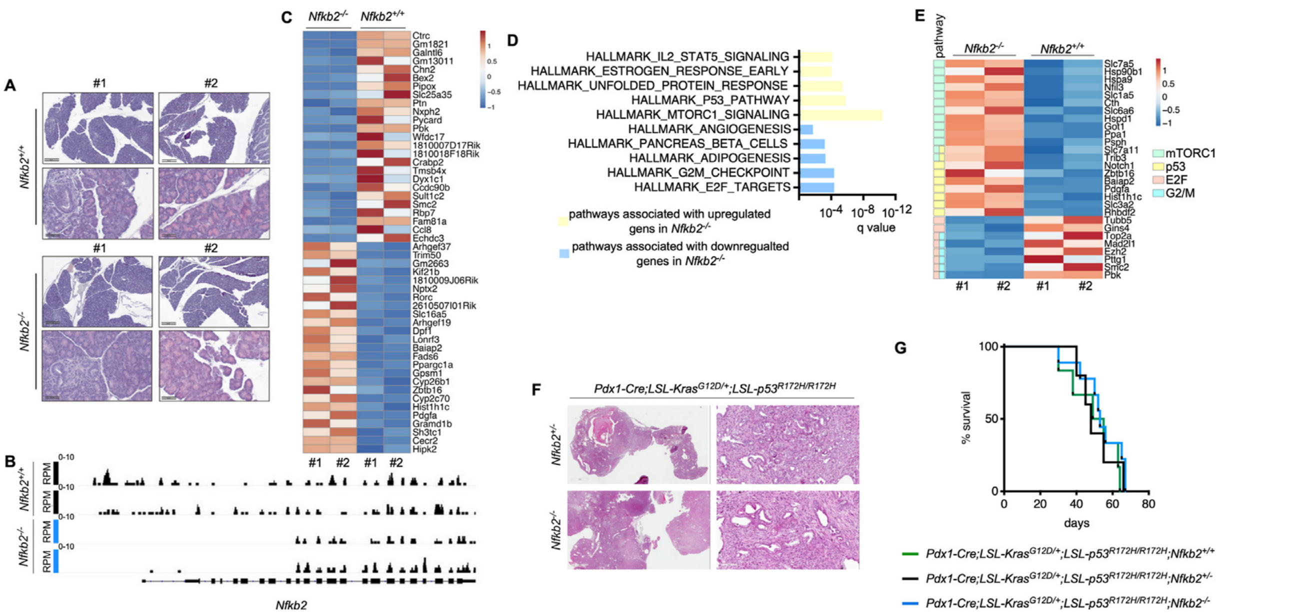

Fig. 4. *Nfκb2 is dispensable in PDAC GEMMs with mutant p53.*
A Representative H&E sections of two four-weeks-old *Pdx1-Cre;LSL-Kras$^{G12D/+}$* and two *Pdx1-Cre;LSL-Kras$^{G12D/+}$; Nfκb2 $^{-/-}$* mice used for RNA-seq analysis (Scale bar: 60 μm and 600 μm). **B** RNA-Seq profiles of two four-weeks-old *Pdx1-Cre;LSL-Kras$^{G12D/+}$* and two *Pdx1-Cre;LSL-Kras$^{G12D/+}$; Nfκb2 $^{-/-}$* mice for the *Nfκb2* locus. mRNA expression is displayed in reads per million mapped reads (RPM). The exon one to nine is not expressed in the knock-out line. **C** Heatmap of the top 50 differential regulated genes in four weeks old *Pdx1-Cre;LSL-Kras$^{G12D/+}$* and *Pdx1-Cre;LSL-Kras$^{G12D/+}$;Nfκb2 $^{-/-}$* mice. **D** Genes up- or down-regulated (log FC ± 1; adj. p value < 0.05) in four weeks old *Pdx1-Cre;LSL-Kras$^{G12D/+}$* and *Pdx1-Cre;LSL-Kras$^{G12D/+}$;Nfκb2 $^{-/-}$* mice were analyzed using the Hallmark Signatures of the Molecular Signature Database. The FDR q value is depicted. **E** Heatmap of genes belonging to the top two up- or down-regulated Hallmark signatures corresponding to D sorted by the q value. The association to the pathways is color coded. **F** Representative H&E sections of *Pdx1-Cre;LSL-Kras$^{G12D/+}$;LSL-p53$^{R172H/R172H}$;Nfκb2$^{+/-}$* (KPPC^{Pdx}N$^{+/-}$) and *Pdx1-Cre;LSL-Kras$^{G12D/+}$;LSL-p53$^{R172H/R172H}$;Nfκb2$^{-/-}$* mice (Scale bar: 2 mm and 100 μm). **G** Kaplan Meier curves of *Pdx1-Cre;LSL-Kras$^{G12D/+}$;LSL-p53$^{R172H/R172H}$;Nfκb2$^{+/+}$* (n = 6; median survival 52 days), *Pdx1-Cre;LSL-Kras$^{G12D/+}$;LSL-p53$^{R172H/R172H}$;Nfκb2$^{+/-}$* (n = 5; median survival 48 days) and *Pdx1-Cre;LSL-Kras$^{G12D/+}$;LSL-p53$^{R172H/R172H}$;Nfκb2$^{-/-}$* (n = 9; median survival 53 days) mice.

Genes linked to the top scoring two Hallmark pathways in each genotype are depicted in Fig. 4E. To further investigate differential activation of p53 in the investigated model, we analyzed the expression of recently described high-confidence p53 target-genes in the RNA-seq dataset [35]. Although some of these genes, including *Cdkn1a*, were expressed at higher levels in KC^{Pdx}N$^{-/-}$ mice, there is a substantial heterogeneity (SFig. 3).

To test a potential genetic interaction of *Nfκb2* with p53, we used a very aggressive PDAC GEMM relying on the simultaneous expression of Kras^{G12D} and the mutated tumor suppressor p53^{R172H} [36]. *Pdx1-Cre;LSL-Kras$^{G12D/+}$;LSL-p53$^{R172H/R172H}$;Nfκb2$^{+/-}$* (KPPC^{Pdx}N$^{+/-}$) as well as *Pdx1-Cre;LSL-Kras$^{G12D/+}$;LSL-p53$^{R172H/R172H}$;Nfκb2$^{-/-}$* (KPPC^{Pdx}N$^{-/-}$) mice develop mPDAC (Fig. 4F). A median survival of 52, 48, and 53 days was observed in KPPC^{Pdx}N$^{+/+}$, KPPC^{Pdx}N$^{+/-}$, and KPPC^{Pdx}N$^{-/-}$, respectively (Fig. 4G). Also *Pdx1-Cre;LSL-Kras$^{G12D/+}$;LSL-p53$^{R172H/+}$;Nfκb2$^{-/-}$* (KPC^{Pdx}N$^{-/-}$) mice develop PDAC and the median survival is not significantly altered compared to KPC^{Pdx}N$^{+/-}$ mice (SFig. 4A and 4B). Western blots of murine PDAC cell lines isolated from p53-mutated cancers document *Nfκb2* knock-out (SFig. 4C). Altogether, *Nfκb2* is dispensable for tumor development in an aggressive murine PDAC model relying on the simultaneous expression of Kras^{G12D} and the p53^{R172H} mutant.

Discussion

Here we show that the *Nfκb2* gene is an important mediator of Kras^{G12D}-driven ADM development and PanIN progression. We reveal that this NFκB family member contributes to proliferation of ADM and PanIN lesions *in vivo*. Furthermore, we demonstrate that *Nfκb2* is dispensable for tumor formation in a p53 mutated PDAC model.

The contribution of NFκB-signaling to the Kras^{G12D}-driven carcinogenesis in the murine pancreas is complex. The canonical pathway, investigated by the use of floxed *RelA* mice, restrains Kras^{G12D}-driven mPanIN progression and tumor development [37]. Mechanistically, RelA seems to contribute to oncogene-induced senescence (OIS) by maintaining the senescence-associated secretory phenotype (SASP) [37]. In models, in which the senescence failsafe is disabled by inactivation of p53, RelA switches to a tumor promoter [37]. We investigated the alternative pathway by the use of *Nfκb2* knock-out mice. The Kras^{G12D}-driven carcinogenesis as well as the proliferative index of ADM and mPanIN cells was impaired in the *Nfκb2*-deficient models. Consistently, inactivation of RelB specifically in the Kras^{G12D} lineage significantly impaired PanIN progression [38]. Together, these data demonstrate at the genetic level that the alternative pathway is needed for Kras^{G12D}-driven carcinogenesis in the murine pancreas, a note supplementarily supported by the description of *Nfκb2* amplifications in PDAC cell lines of KC mice [5]. Although we detected impaired proliferation in the investigated model, we currently cannot exclude the contribution of other processes to the observed phenotype.

Cross-talk of wildtype p53 with the NFκB-p52 subunit involving different molecular mechanisms, which involves interaction of both proteins and agonistic as well as antagonistic effects of p52 to p53 target gene expression, is documented [39–42]. Although our genetic data demonstrate that the tumor promoting function of *Nfκb2* in the carcinogenesis in the pancreas is dispensable in case that p53 is mutated, the molecular mechanisms are currently unclear and need further experimentations, best in models with reduced complexity. Furthermore, we cannot conclude from the data that a cross-talk of wildtype p53 with NFκB-p52 is operative and contributes to the observed phenotypes.

In pancreatic cancer cells, cell-autonomous functions of noncanonical NFκB-signaling for proliferation and the cell cycle in the pancreatic context were shown [18–21]. Experiments conducted with floxed *RelB* mice in the KC model, showed a cell intrinsic function of alternative NFκB-signaling during the carcinogenesis in the pancreas [38]. Although there is a phenotypic overlap in the *RelB*- and *Nfκb2*-deficient pancreatic cancer models, we cannot exclude that cell non-autonomous functions contribute or were mainly responsible for the observed phenotype due to the complete *Nfκb2* knock-out mouse line used in our analysis. Pancreatic cancer initiation and progression is modulated by a sophisticated fibroinflammatory microenvironment [43–46]. Therefore, a role of the *Nfκb2* gene in non-epithelial cells could also contribute to the described phenotype. Deciphering of compartment-specific functions of the *Nfκb2* gene demand the use of conditional *Nfκb2* mice [47] and advanced pancreatic cancer models [24].

With *Zeb1* [48] or *Egfr* [49,50], *Nfκb2* belongs to a spectrum of genes demonstrating variable impact on disease progression in solely $Kras^{G12D}$-driven PDAC models versus models depending on the simultaneous inactivation of p53 and expression of $Kras^{G12D}$. Such data demonstrate the highly context dependent requirements of oncogenic signaling [51]. Deciphering the molecular mechanisms of context specific signaling will increase our understanding of the genetic hallmarks of tumors.

Author contributions

Study Concept and Design: Z.H., C.S., R.S., O.H.K., R.R., C.G., A.A., M.S., D.S., and G.S.; Acquisition of Data: Z.H., C.S., M.W., S.M., K.S. and T.N.; Analysis and Interpretation of Data: All authors; Drafting of the Manuscript and Critical Revision of the Manuscript for Important Intellectual Content: All authors; Final Approval of the Submitted Manuscript: All authors.

Acknowledgement

We thank all colleagues providing mouse lines. This work was supported by the Wilhelm-Sander Foundation [2017.048.2 to G.S. and 2019.086.1 to G.S. and O.H.K], Deutsche Forschungsgemeinschaft (DFG) [SCHN 959/3-2 and SCHN959/6-1 to G.S. and SFB1321 (Project-ID 329628492) P13 to G.S. and S01 to K.S., G.S., M.R., R.R. and D.S], Deutsche Krebshilfe [70113760 to G.S. and 111273 (Max-Eder Program) to M.R.]. *Conflict of Interest: Nothing to disclose.*

Appendix A. Supplementary data

Supplementary data to this article can be found online at https://doi.org/10.1016/j.pan.2021.03.012.

References

[1] Schneeweis C, Wirth M, Saur D, Reichert M, Schneider G. Oncogenic kras and the egfr loop in pancreatic carcinogenesis-a connection to licensing nodes. Small GTPases 2016:1–8.
[2] Eser S, Schnieke A, Schneider G, Saur D. Oncogenic kras signalling in pancreatic cancer. Br J Canc 2014;111:817–22.
[3] Buscail L, Bournet B, Cordelier P. Role of oncogenic kras in the diagnosis, prognosis and treatment of pancreatic cancer. Nat Rev Gastroenterol Hepatol 2020;17:153–68.
[4] Lanfredini S, Thapa A, O'Neill E. Ras in pancreatic cancer. Biochem Soc Trans 2019;47:961–72.
[5] Mueller S, Engleitner T, Maresch R, Zukowska M, Lange S, Kaltenbacher T, et al. Evolutionary routes and kras dosage define pancreatic cancer phenotypes. Nature 2018;554:62–8.
[6] Chan-Seng-Yue M, Kim JC, Wilson GW, Ng K, Figueroa EF, O'Kane GM, et al. Transcription phenotypes of pancreatic cancer are driven by genomic events during tumor evolution. Nat Genet 2020;52:231–40.
[7] Hayden MS, Ghosh S. Nf-kappab, the first quarter-century: remarkable progress and outstanding questions. Genes Dev 2012;26:203–34.
[8] Zhang Q, Lenardo MJ, Baltimore D. 30 years of nf-kappab: a blossoming of relevance to human pathobiology. Cell 2017;168:37–57.
[9] Mulero MC, Huxford T, Ghosh G. Nf-kappab, ikappab, and ikk: integral components of immune system signaling. Adv Exp Med Biol 2019;1172:207–26.
[10] Prabhu L, Mundade R, Korc M, Loehrer PJ, Lu T. Critical role of nf-kappab in pancreatic cancer. Oncotarget 2014;5:10969–75.
[11] Storz P. Targeting the alternative nf-kappab pathway in pancreatic cancer: a new direction for therapy? Expert Rev Anticancer Ther 2013;13:501–4.
[12] Geismann C, Schäfer H, Gundlach JP, Hauser C, Egberts JH, Schneider G, et al. Nf-kappab dependent chemokine signaling in pancreatic cancer. Cancers (Basel) 2019:11.
[13] Kabacaoglu D, Ruess DA, Ai J, Algul H. Nf-kappab/rel transcription factors in pancreatic cancer: focusing on rela, c-rel, and relb. Cancers (Basel) 2019;11.
[14] Li Q, Yang G, Feng M, Zheng S, Cao Z, Qiu J, et al. Nf-kappab in pancreatic cancer: its key role in chemoresistance. Canc Lett 2018;421:127–34.
[15] Khurana N, Dodhiawala PB, Bulle A, Lim KH. Deciphering the role of innate immune nf-kb pathway in pancreatic cancer. Cancers (Basel) 2020;12.
[16] Maier HJ, Wagner M, Schips TG, Salem HH, Baumann B, Wirth T. Requirement of nemo/ikkgamma for effective expansion of kras-induced precancerous lesions in the pancreas. Oncogene 2013;32:2690–5.
[17] Ling J, Kang Y, Zhao R, Xia Q, Lee DF, Chang Z, et al. Krasg12d-induced ikk2/beta/nf-kappab activation by il-1alpha and p62 feedforward loops is required for development of pancreatic ductal adenocarcinoma. Canc Cell 2012;21:105–20.
[18] Doppler H, Liou GY, Storz P. Downregulation of traf2 mediates nik-induced pancreatic cancer cell proliferation and tumorigenicity. PLoS One 2013;8:e53676.
[19] Bang D, Wilson W, Ryan M, Yeh JJ, Baldwin AS. Gsk-3alpha promotes oncogenic kras function in pancreatic cancer via tak1-tab stabilization and regulation of noncanonical nf-kappab. Canc Discov 2013;3:690–703.
[20] Schneider G, Saur D, Siveke JT, Fritsch R, Greten FR, Schmid RM. Ikkalpha controls p52/relb at the skp2 gene promoter to regulate g1- to s-phase progression. EMBO J 2006;25:3801–12.
[21] Nishina T, Yamaguchi N, Gohda J, Semba K, Inoue J. Nik is involved in constitutive activation of the alternative nf-kappab pathway and proliferation of pancreatic cancer cells. Biochem Biophys Res Commun 2009;388:96–101.
[22] Paxian S, Merkle H, Riemann M, Wilda M, Adler G, Hameister H, et al. Abnormal organogenesis of peyer's patches in mice deficient for nf-kappab1, nf-kappab2, and bcl-3. Gastroenterology 2002;122:1853–68.
[23] Diersch S, Wirth M, Schneeweis C, Jors S, Geisler F, Siveke JT, et al. Kras(g12d) induces egfr-myc cross signaling in murine primary pancreatic ductal epithelial cells. Oncogene 2016;35:3880–6.
[24] Schönhuber N, Seidler B, Schuck K, Veltkamp C, Schachtler C, Zukowska M, et al. A next-generation dual-recombinase system for time- and host-specific targeting of pancreatic cancer. Nat Med 2014;20:1340–7.
[25] Eser S, Reiff N, Messer M, Seidler B, Gottschalk K, Dobler M, et al. Selective requirement of pi3k/pdk1 signaling for kras oncogene-driven pancreatic cell plasticity and cancer. Canc Cell 2013;23:406–20.
[26] Hassan Z, Schneeweis C, Wirth M, Veltkamp C, Dantes Z, Feuerecker B, et al. Mtor inhibitor-based combination therapies for pancreatic cancer. Br J Canc 2018;118:366–77.
[27] Diersch S, Wenzel P, Szameitat M, Eser P, Paul MC, Seidler B, et al. Efemp1 and p27(kip1) modulate responsiveness of pancreatic cancer cells towards a dual pi3k/mtor inhibitor in preclinical models. Oncotarget 2013;4:277–88.
[28] Hruban RH, Adsay NV, Albores-Saavedra J, Anver MR, Biankin AV, Boivin GP, et al. Pathology of genetically engineered mouse models of pancreatic exocrine cancer: consensus report and recommendations. Canc Res 2006;66:95–106.
[29] von Burstin J, Eser S, Paul MC, Seidler B, Brandl M, Messer M, et al. E-cadherin regulates metastasis of pancreatic cancer in vivo and is suppressed by a snail/hdac1/hdac2 repressor complex. Gastroenterology 2009;137:361–71. 371 e361-365.
[30] Ossewaarde JM, de Vries A, Bestebroer T, Angulo AF. Application of a mycoplasma group-specific pcr for monitoring decontamination of mycoplasma-infected chlamydia sp. Strains. Appl Environ Microbiol 1996;62:328–31.
[31] Metsalu T, Vilo J, Clustvis. A web tool for visualizing clustering of multivariate data using principal component analysis and heatmap. Nucleic Acids Res 2015;43:W566–70.
[32] Rodolosse A, Chalaux E, Adell T, Hagege H, Skoudy A, Real FX. Ptf1alpha/p48 transcription factor couples proliferation and differentiation in the exocrine pancreas [corrected]. Gastroenterology 2004;127:937–49.
[33] Krah NM, De La OJ, Swift GH, Hoang CQ, Willet SG, Chen Pan F, et al. The acinar differentiation determinant ptf1a inhibits initiation of pancreatic ductal adenocarcinoma. Elife 2015;4.
[34] Tegowski M, Baldwin A. Noncanonical nf-kappab in cancer. Biomedicines 2018;6.
[35] Fischer M. Census and evaluation of p53 target genes. Oncogene 2017;36:3943–56.
[36] Hingorani SR, Wang L, Multani AS, Combs C, Deramaudt TB, Hruban RH, et al. Trp53r172h and krasg12d cooperate to promote chromosomal instability and widely metastatic pancreatic ductal adenocarcinoma in mice. Canc Cell 2005;7:469–83.
[37] Lesina M, Wormann SM, Morton J, Diakopoulos KN, Korneeva O, Wimmer M, et al. Rela regulates cxcl1/cxcr2-dependent oncogene-induced senescence in murine kras-driven pancreatic carcinogenesis. J Clin Invest 2016;126:

2919–32.
[38] Hamidi T, Algul H, Cano CE, Sandi MJ, Molejon MI, Riemann M, et al. Nuclear protein 1 promotes pancreatic cancer development and protects cells from stress by inhibiting apoptosis. J Clin Invest 2012;122:2092–103.
[39] Iannetti A, Ledoux AC, Tudhope SJ, Sellier H, Zhao B, Mowla S, et al. Regulation of p53 and rb links the alternative nf-kappab pathway to ezh2 expression and cell senescence. PLoS Genet 2014;10:e1004642.
[40] Schumm K, Rocha S, Caamano J, Perkins ND. Regulation of p53 tumour suppressor target gene expression by the p52 nf-kappab subunit. EMBO J 2006;25:4820–32.
[41] Rocha S, Martin AM, Meek DW, Perkins ND. P53 represses cyclin d1 transcription through down regulation of bcl-3 and inducing increased association of the p52 nf-kappab subunit with histone deacetylase 1. Mol Cell Biol 2003;23:4713–27.
[42] Furth N, Bossel Ben-Moshe N, Pozniak Y, Porat Z, Geiger T, Domany E, et al. Down-regulation of lats kinases alters p53 to promote cell migration. Genes Dev 2015;29:2325–30.
[43] Zhang Y, Crawford HC, Pasca di Magliano M. Epithelial-stromal interactions in pancreatic cancer. Annu Rev Physiol 2018;81:211–33.
[44] Neesse A, Algul H, Tuveson DA, Gress TM. Stromal biology and therapy in pancreatic cancer: a changing paradigm. Gut 2015;64:1476–84.
[45] Huber M, Brehm CU, Gress TM, Buchholz M, Alashkar Alhamwe B, von Strandmann EP, et al. The immune microenvironment in pancreatic cancer. Int J Mol Sci 2020;21.
[46] Hessmann E, Buchholz SM, Demir IE, Singh SK, Gress TM, Ellenrieder V, et al. Microenvironmental determinants of pancreatic cancer. Physiol Rev 2020;100:1707–51.
[47] De Silva NS, Anderson MM, Carette A, Silva K, Heise N, Bhagat G, et al. Transcription factors of the alternative nf-kappab pathway are required for germinal center b-cell development. Proc Natl Acad Sci U S A 2016;113:9063–8.
[48] Krebs AM, Mitschke J, Lasierra Losada M, Schmalhofer O, Boerries M, Busch H, et al. The emt-activator zeb1 is a key factor for cell plasticity and promotes metastasis in pancreatic cancer. Nat Cell Biol 2017;19:518–29.
[49] Navas C, Hernandez-Porras I, Schuhmacher AJ, Sibilia M, Guerra C, Barbacid M. Egf receptor signaling is essential for k-ras oncogene-driven pancreatic ductal adenocarcinoma. Canc Cell 2012;22:318–30.
[50] Ardito CM, Gruner BM, Takeuchi KK, Lubeseder-Martellato C, Teichmann N, Mazur PK, et al. Egf receptor is required for kras-induced pancreatic tumorigenesis. Canc Cell 2012;22:304–17.
[51] Schneider G, Schmidt-Supprian M, Rad R, Saur D. Tissue-specific tumorigenesis: context matters. Nat Rev Canc 2017;17:239–53.